Available online at www.sciencedirect.com
SCIENCE DIRECT®
Journal of Nuclear Materials 337–339 (2005) 166–170
journal of nuclear materials
www.elsevier.com/locate/jnucmat

Experimental study of negative ion profiles in H_2-MAR plasmas in divertor simulator MAP-II

S. Kado [a,*], S. Kajita [b], D. Yamasaki [b], Y. Iida [b], B. Xiao [c], T. Shikama [b], T. Oishi [b], A. Okamoto [a], S. Tanaka [b]

[a] *High Temperature Plasma Center, The University of Tokyo, 2-11-16 Yayoi, Bunkyo-ku, Tokyo 113-8656, Japan*
[b] *Graduate School of Engineering, The University of Tokyo, Japan*
[c] *Institute of Plasma Physics, Chinese Academy of Sciences, China*

Abstract

The negative hydrogen ion density profile is measured in hydrogen molecular assisted recombination (MAR) plasmas in the steady-state linear divertor/edge plasma simulator material and plasma (MAP)-II device. Fulcher band spectroscopy is also performed for the measurement of the ro-vibrational distribution of hydrogen molecules and the degree of dissociation. We have developed negative ion diagnostics using a combined scheme of an 'eclipse' laser photo-detachment system and a double probe. The former is to avoid probe surface ablation phenomena while the latter is to avoid the anomaly in the Langmuir probe characteristics in recombining plasmas, which leads to an overestimation of T_e. Negative hydrogen ions are detected in the peripheral regions of the hot plasma column while vibrationally excited molecules exist in the plasma core. Based on the rate equation, the measured negative ion density is compared with the results of model calculations.

PACS: 52.75; 39.30; 32.80.G; 33.15.F
Keywords: Divertor plasma; Molecular effects; Recombination; Spectroscopy; MAP-II

1. Introduction

The enhancement of volumetric recombination processes in divertor/edge plasmas has been regarded as being a potentially important scenario in reducing particle and heat flux onto the plasma-facing components [1]. In past studies, we have investigated volumetric recombination processes in a steady-state linear divertor/edge plasma simulator material and plasma (MAP)-II device. Electron-ion recombination (EIR), represented by three-body and radiative recombination processes [2], and molecular-activated/assisted recombination (MAR), caused by the hydrogen or hydrocarbon [3] molecules, are of interest with regard to the electron temperature regime in which the individual processes dominate the reduction of particle/heat flux.

Qualitatively, the indication of the MAR occurring through negative ion channels has been observed in the divertor simulator TPD-IVSHEET [4]. Our previous work has shown that under 'attached' conditions, the negative ion density first increases with the hydrogen neutral pressure, and then begins to decrease due to the decrease of the vibrational temperature, which may

* Corresponding author. Tel.: +81 3 5841 7667; fax: +81 3 5802 7221.
E-mail address: kado@q.t.u-tokyo.ac.jp (S. Kado).

0022-3115/$ - see front matter © 2004 Elsevier B.V. All rights reserved.
doi:10.1016/j.jnucmat.2004.10.142

be caused by the reduction in the electron energy [5]. When extending this experiment to 'detached' conditions, however, quantitative analyses are difficult to perform because the T_e measurement using a Langmuir probe, and as a consequence, the n_e value, is disturbed in the recombining plasmas [6,7]. Therefore, the development of diagnostics for the purpose of studying recombining plasma with higher reliability is important.

In the present paper, newly developed diagnostics are applied to recombining plasmas and the initial results obtained in the MAP-II recombining plasmas are presented.

2. Diagnostics for the recombining plasmas

2.1. Combined scheme of eclipse laser photo-detachment and double probe

In order to measure negative ion density, we have installed a laser photo-detachment (LPD) system combined with a positively biased L-shaped electrostatic probe [8]. We have noticed two major problems in the application of LPD to high-density recombining plasmas, namely the ablation phenomena of the probe surface adsorbates [9] and an anomaly that appears in the single probe characteristics.

Although the ablation can be detected by means of a negatively biased probe [9], we have developed an ablation-free technique, called Eclipse-LPD [10], as shown in Fig. 1. A thin wire is installed in the laser channel to shield the probe tip from the irradiation of the laser pulse, just as the earth shields the moon from the irradiation of the sunlight during the lunar eclipse.

For the purpose of compensating the single probe anomaly, we have introduced the following more direct representation of the relationship between the excess

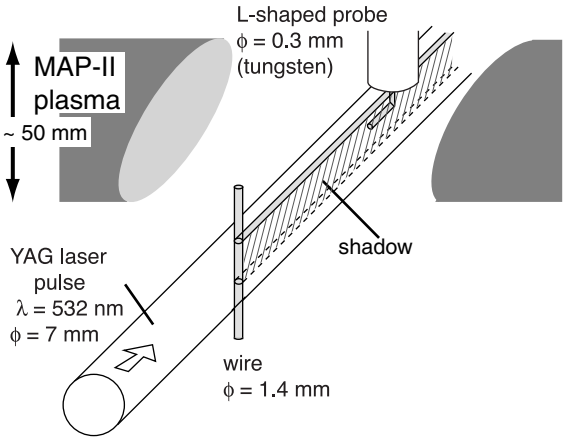

Fig. 1. The concept of the eclipse laser photo-detachment technique.

electron density due to the photo-detachment, Δn_e, at the space potential, V_s (=negative ion density), and the excess electron current, ΔI_e, at the probe voltage, V_p, as

$$\frac{\Delta I_e(V_p)}{I_e(V_p)} = \frac{\frac{eS}{4}\Delta n_e\sqrt{8kT_e/\pi m_e}}{I_e(V_s)}, \quad (1)$$

where S is the probe surface area, T_e in the equation is measured by a double probe at the same position. It has been reported that the double probe provides more reliable values in detached recombining plasmas [7]. Eq. (1) is implicitly based on the assumption that the dependence of the degree of electron current reduction due to the plasma impedance and that due to the potential bursts [7] on the probe bias voltage are equal, even though both of the values at V_p and V_s exhibit anomalies. On the other hand, the reduction of the excess electron current is negligible, since the collection area for the photo-detached electrons is smaller than the laser radius in our experimental regime [11].

2.2. Spectroscopy for H_2-Fulcher band and hydrogen Balmer series

We have developed an analysis scheme for Fulcher-α band ($d^3\Pi_u - a^3\Sigma_g$) spectra from H_2 molecules in order to determine the vibrational and rotational Boltzmann temperatures, T_{vib} and T_{rot} respectively, in the ground electronic state ($X^1\Sigma_g$) [12]. Ro-vibrational structure in the excitation rate is evaluated from the adiabatic approximation combined with Gryzinski's semi-classical electron exchange cross-sections [13].

A collisional–radiative (CR) model is applied to the H atom. The code is the simplest one in which only hydrogen atoms can be treated. The dissociative excitation rate of H_2 scales to n^{-6} while direct electron impact excitation rate of H atoms scales to n^{-3} where n is the principal quantum number [14]. This suggests that the molecular contribution to the Balmer series emission decreases as n increases. Therefore, the ratio of H atomic to H_2 molecular densities is evaluated from the ratio of photon fluxes, ε, of H_δ to the Fulcher α, namely,

$$\frac{\varepsilon(H_\delta)}{\varepsilon(H_2(d\rightarrow a))} = \frac{[H]X^{eff}_{1\rightarrow 6}(n_e,T_e)B(H_\delta)}{n_e[H_2]X_{d\leftarrow X}(T_e)}, \quad (2)$$

where $X^{eff}_{1\rightarrow 6}(n_e,T_e)$ is the effective cross-section for populating to the $n = 6$ state of the hydrogen atom, $B(H_\delta)$ is the branching ratio of the radiative transition and $X_{d\leftarrow X}(T_e)$ is the total excitation rate of the Fulcher band based on the coronal model [12].

3. Results and discussion

Plasmas are generated in an arc source region between a flat LaB_6 cathode disk and an anode pipe of

the steady-state linear divertor/edge plasma simulator MAP-II device. A core plasma stream with a diameter of about 5 cm is transmitted along a longitudinal magnetic field of about 0.015–0.02 T, passing through a first chamber (source chamber) into a second chamber (gas target chamber located at a distance of 1.5 m from the plasma source), and finally terminated at the floating target plate. A 'detached' condition can be achieved by turning off the differential evacuation of the source chamber as described in Ref. [3]. A small amount of hydrogen gas is seeded in the plasma source for diagnostic purposes. Then, H_2 is puffed into the target chamber. The ratio of hydrogen gas to background helium is estimated from the total pressure and the variation of the helium partial pressure obtained using a quadrapole mass analyzer. This calculation is necessary because of the dependence of the pumping speed of the turbo molecular pump on the total pressure.

A 1 m Czerny–Turner scanning monochromator equipped with a 2400 grooves/mm holographic grating and a photo-multiplier tube (PMT) detector is used for the optical measurements. The typical wavelength resolution in the present work is less than 0.03 nm at a 50 μm slit width.

In this series of experiments, a probe for LPD was located at the center of the target chamber where the sightline of the spectroscopy was situated. The discharge voltage and current were 71 V and 30 A, respectively.

The contour plot of the negative ion density versus radial position (vertical axis) and pressure (horizontal axis) at the target chamber is shown in Fig. 2(a). The various total pressure conditions (H_2 flow rate to the target chamber, sccm) are 3.1 (6), 4.5 (33), 5.7 (67), 7.4 (100), 9.0 (133), 11.7 (167) and 14.4 (200) mTorr. The negative ion density is localized in the peripheral region of the hot plasma core having a maximum value around 5 cm, and the value decreases as the pressure increases, as shown in Fig. 2(b). T_e and n_e profiles for 4.5 and 9.0 mTorr are shown in Figs. 2(c) and (d), respectively.

Fig. 3 shows the dependence of the measured parameters on the gas pressure. The remarkable decrease in the ion saturation current (a) as the hydrogen gas increases indicates the onset of MAR processes. This was previously described in [3] where a comparative investigation was made between the case of He, H_2 and hydrocarbon puffing into the He background plasma stream. The decay rate of the negative ions around the peak area is similar to that of the ion flux. Since the electron temperature does not change, the ion flux reduction corresponds to an electron density decay. This observation indicates that the ratio of the negative ion density to the electron density does not change during this MAR phase. Rydberg series spectra of He I and H I, which are typical for the EIR case of $T_e < 0.1$ eV, cannot be observed in these conditions [2].

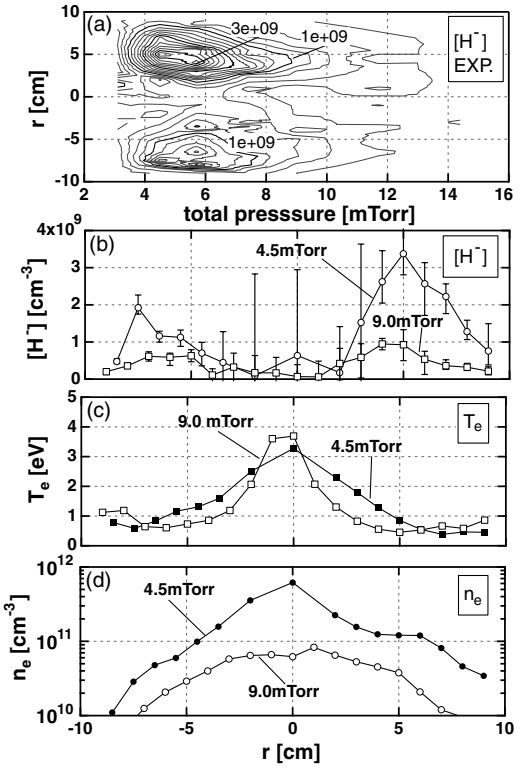

Fig. 2. (a) Contour plot of the measured negative ion density profile as a function of the total neutral pressure. Radial profiles of (b) the negative ion density, (c) the electron temperature and (d) the electron density for 4.5 and 9.0 mTorr.

The negative ion density is evaluated from a steady state solution of the following simple rate equation [5]:

$$n_{H^-} = n_e \sum_{0 \leqslant v \leqslant 9} \alpha_{e,H_2} n_{H_2(v)} / (n_e \alpha_{e,H^-} + n_{H^+} \alpha_{H^+,H^-} + 1/\tau), \quad (3)$$

where α_{e,H_2}, α_{H^+,H^-} and α_{e,H^-} are the rate coefficients for dissociative attachment (DA), mutual neutralization (MN) and electron impact detachment, respectively [15–17]. We assumed in the equation that the vibrational distribution of H_2 in the ground electronic state is Boltzmann, and that the MN rate for H_2^+ and He^+ is equal to that of H^+. We neglect the contribution of τ for simplicity and discuss it later. Measured n_e and T_e profiles are used as the input parameters. The H_2 density in the plasma column is estimated based on the partial pressure of the working gas and the degree of dissociation of hydrogen molecules deduced from the Fulcher–Balmer ratio as described in Eq. (2). The contour plot of the result is shown in Fig. 4(a). The radial profile of the production and loss rate of negative ions at 4.5 mTorr is shown in Fig. 4(b).

As seen from the comparison between Figs. 2(b) and 4(c), the radial profile of the measured negative ion density is reproduced for 4.5 mTorr, while the calculation

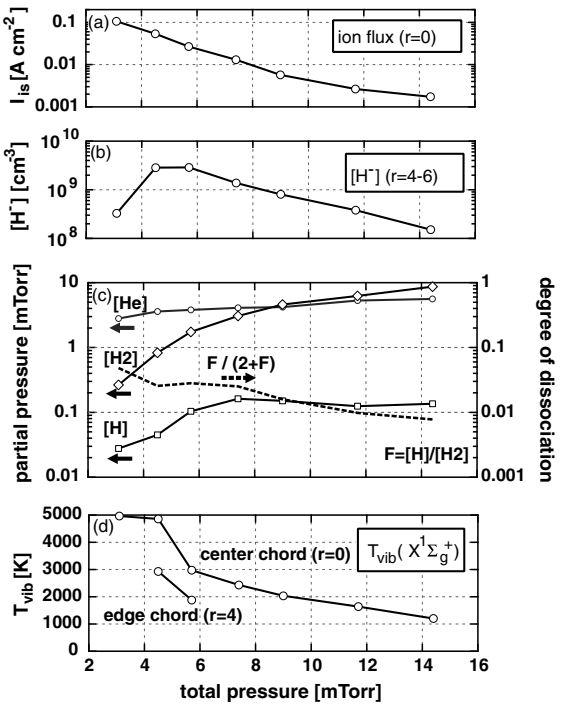

Fig. 3. Pressure dependence of (a) the ion saturation current at $r = 0$ cm, (b) the negative ion density averaged over $r = 4$–6 cm, (c) the partial pressure of the He, H_2 and H together with the degree of dissociation and (d) the vibrational temperature for central and edge chords.

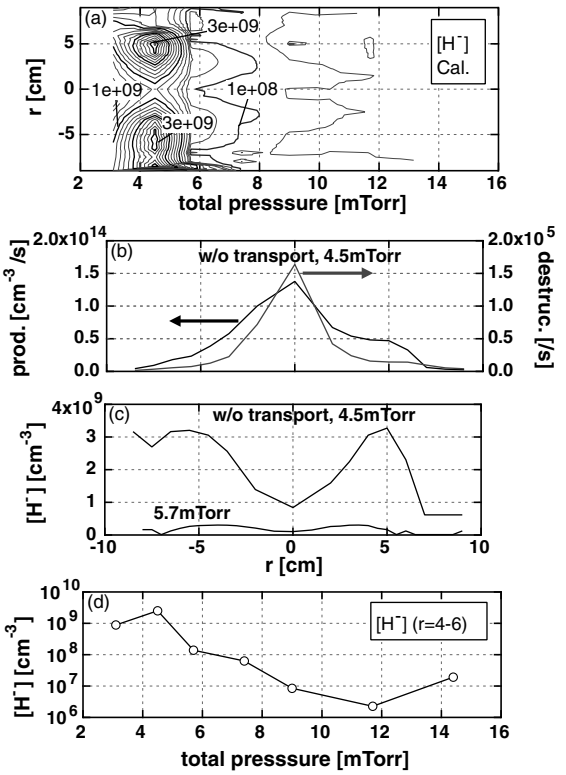

Fig. 4. (a) Contour plot of the calculated negative ion density profile as a function of the total neutral pressure. Radial profiles are shown for (b) the production and destruction rates for 4.5 mTorr and (c) the negative ion density for 4.5 and 5.7 mTorr. (d) Pressure dependence of the calculated negative ion density averaged over $r = 4$–6 cm.

results show considerably lower density as the pressure increases, as seen in Fig. 4(d).

Fig. 4(b) indicates that both the production and loss processes occur in the plasma core rather than in the periphery where negative ions exist. However, since the region of the depletion process, where T_e is rather high, is narrower than that of the production processes, the negative ions in the peripheral region escape destruction. The production rate is calculated using the T_{vib} measured in the central chord. The T_{vib} at the plasma edge 4 cm from the center, shown in Fig. 3(d), is so low that those molecules are not able to contribute to the negative ion production. Note that the emission from the central chord cannot be influenced by the edge Fulcher emission because the emissivity from the periphery is too small. Therefore, the negative ions observed in the peripheral region around $r = 4$ cm are regarded as being produced in the inner region and then escaping to the periphery without encountering the destruction/depletion processes. The lifetime of the negative ions estimated from the reciprocal of the destruction rate is about 10 μs while the drift velocity of the negative ions is on the order of several kilometers/second, yielding a travel length of about several cm, which does not contradict the observations.

However, it is difficult to explain the discrepancy in the pressure dependence of the absolute value of the negative ion density. The calculated values decrease more rapidly than the experimental ones as the pressure increases. One possible reason for this discrepancy is the transport of the negative ions in the present conditions. If the transport loss time scale is considered in Eq. (3), then the calculated negative ion density becomes lower. This may be true in the central region where almost no negative ions can be observed. On the other hand, in the plasma periphery, even though the production is negligible due to the low vibrational temperature, the negative ion flux that escaped from the central region without being destroyed by MN and detachment processes should be superposed. Roughly, if a typical transport rate from the center to the edge region of about 10^4 s^{-1} is added, then the negative ion density for, say, 5.7 mTorr becomes comparable to that observed experimentally. Kinetic treatments or particle simulations are necessary for more qualitative discussions including the radial profiles of the production, destruction and transport effects. These topics will be subjects of study in the future.

Another possible reason for the discrepancy is the departure from a Boltzmann distribution of the vibrational distribution function in the ground electronic state of the hydrogen molecules. As can be understood from the Franck–Condon factors for the X–d excitation in the H_2 molecule, the Fulcher-α band is sensitive to the vibrational distribution for $v \leqslant 4$, while the main contributor to the negative ion production is the population in $v \geqslant 4$. Therefore, if a 'tail', 'bi-Maxwellian' or 'plateau' region exists in the vibrational distribution in the ground electronic state, the production cannot be predicted from the Fulcher band spectroscopy on the basis of the T_{vib}. Our kinetic modeling for the mechanism of the vibrational distribution [18], as well as several calculations and LIF measurements [19], indicates a departure from a Boltzmann distribution.

4. Summary

We have developed diagnostics for the study of volumetric recombination plasmas: (i) a combined scheme of eclipse laser photo-detachment technique and double probe diagnostics, and (ii) optical measurements for Fulcher and Balmer emission.

Under hydrogen-MAR conditions in MAP-II device the level of the negative ions in the plasma periphery is higher than that predicted based on the rate equation, even without considering transport loss. The hypothesis to explain this observation is that the negative ions are produced in the plasma core where the vibrational temperature is relatively high, and then transported to the periphery where the production of the negative ions is impossible due to low vibrational temperature.

References

[1] S.I. Krasheninnikov, A.Yu. Pigarov, D.J. Sigmar, Phys. Lett. A 214 (1996) 285.
[2] S. Kado, S. Kajita, Y. Iida, B. Xiao, T. Shikama, D. Yamasaki, T. Oishi, S. Tanaka, J. Plasma, Sci. Technol. 6 (2004) 2451.
[3] S. Kado, H. Kobayashi, T. Oishi, S. Tanaka, J. Nucl. Mater. 313–316 (2003) 754.
[4] A. Tonegawa, M. Ono, Y. Morihira, H. Ogawa, T. Shibuya, K. Kawamura, K. Takayama, J. Nucl. Mater. 313–316 (2003) 1046.
[5] S. Kajita, S. Kado, N. Uchida, T. Shikama, S. Tanaka, J. Nucl. Mater. 313–316 (2003) 748.
[6] R.D. Monk et al., J. Nucl. Mater. 241–243 (1997) 396.
[7] N. Ohno et al., Contrib. Plasma Phys. 41 (5) (2001) 473.
[8] M. Bacal, G.W. Hamilton, A.M. Bruneteau, H.J. Doucet, Rev. Sci. Instrum. 50 (1979) 719.
[9] S. Kajita, S. Kado, T. Shikama, B. Xiao, S. Tanaka, Contrib. Plasma Phys. 44 (2004) 607.
[10] S. Kajita, S. Kado, A. Okamoto, T. Shikana, B. Xiao, Y. Iida, D. Yamasaki, S. Tanaka, Proc. EPS Conference on Plasma Physics, London, 2004, P-2.123.
[11] S. Kajita, S. Kado, A. Okamoto, S. Tanaka, Phys. Rev. E 70 (6) (2004) 066403.
[12] B. Xiao, S. Kado, S. Kajita, D. Yamasaki, Plasma Phys. Control. Fus. 46 (2004) 653.
[13] M. Gryzinski, Phys. Rev. 138 (1965) A336.
[14] T. Fujimoto, K. Sawada, K. Takahata, J. Appl. Phys. 66 (1989) 2315.
[15] R. Celiberto, R.K. Janev, A. Laricchiuta, M. Capitelli, J.M. Wadehra, D.E. Atems, At. Data Nucl. Data Tables 77 (2001) 161.
[16] J.M. Wadehra, Appl. Phys. Lett. 35 (1979) 917.
[17] R.K. Janev, W.D. Langer, et al., Elementary Processes in Hydrogen–Helium Plasmas, Springer, Berlin, 1987.
[18] B. Xiao, S. Kado, S. Kajita, D. Yamasaki, S. Tanaka, these Proceedings. doi:10.1016/j.jnucmat.2004.10.025.
[19] T. Mosbach, H.M. Katsch, H.F. Döbele, Phys. Rev. Lett. 85 (2000) 3420.